Nanoscale

RSC Publishing

PAPER

Functionalization of PEGylated Fe_3O_4 magnetic nanoparticles with tetraphosphonate cavitand for biomedical application

Cite this: *Nanoscale*, 2013, **5**, 11438

C. Tudisco,[a] F. Bertani,[b] M. T. Cambria,[a] F. Sinatra,[c] E. Fantechi,[d] C. Innocenti,[d] C. Sangregorio,[de] E. Dalcanale[b] and G. G. Condorelli*[a]

Received 30th April 2013
Accepted 4th August 2013

DOI: 10.1039/c3nr02188b

www.rsc.org/nanoscale

In this contribution, Fe_3O_4 magnetic nanoparticles (MNPs) have been functionalized with a tetraphosphonate cavitand receptor (Tiiii), capable of complexing *N*-monomethylated species with high selectivity, and polyethylene glycol (PEG) *via* click-chemistry. The grafting process is based on MNP pre-functionalization with a bifunctional phosphonic linker, 10-undecynylphosphonic acid, anchored on an iron surface through the phosphonic group. The Tiiii cavitand and the PEG modified with azide moieties have then been bonded to the resulting alkyne-functionalized MNPs through a "click" reaction. Each reaction step has been monitored by using X-ray photoelectron and FTIR spectroscopies. PEG and Tiiii functionalized MNPs have been able to load *N*-methyl ammonium salts such as the antitumor drug procarbazine hydrochloride and the neurotransmitter epinephrine hydrochloride and release them as free bases. In addition, the introduction of PEG moieties promoted biocompatibility of functionalized MNPs, thus allowing their use in biological environments.

Introduction

Magnetic nanoparticles (MNPs) have attracted enormous attention for their potential use in the biomedical field for both diagnostic and therapeutic applications[1,2] such as controlled drug delivery,[3] cell separation,[4] magnetic resonance imaging (MRI),[5,6] localized hyperthermia for cancer therapy (MFH),[7] biosensing[8] and detoxification of biological fluids.[9,10] The intrinsic multifunctionality due to the combination of superparamagnetic properties with biocompatibility and biological activity provided by the specific coatings of the superparamagnetic core is the most attractive aspect of MNPs. The search for new MNPs pointed to two objectives: the improvement of the efficiency of the superparamagnetic core[11] and the development of versatile, active and stable coatings which represent the functional interface between MNPs and the biological environment.[12–14] Since the surface plays a pivotal role in determining the interaction between the MNP and its biological target, the quality of the functionalization of the MNP surface is crucial to a successful application in the biological field. For this reason, the present decade has seen a surge of interest in functionalization studies of magnetic metal oxides with biocompatible coatings such as PEG,[15] cyclodextrins,[16] and dextrane[17] based on polymeric films or on covalently bonded molecular monolayers[18–22] usually acting as a linker between the surface and the active molecules.

In this context, we describe the synthesis of new multifunctional organic–inorganic MNPs, which possess suitable biocompatibility and magnetic properties, and are designed to load, carry and release *N*-methylated drugs and biomolecules. The synthesized MNPs consist of a Fe_3O_4 core covalently coated with a mixed monolayer of PEG and tetraphosphonate cavitand. The key strength of the new system lies in the highly selective recognition properties of the tetraphosphonate cavitands (Tiiii) towards *N*-methyl ammonium salts. Cavitands, synthetic organic compounds with resorcinarene-based cavities of molecular dimensions, are well-known molecular receptors,[23] and, in particular, the complexation properties of Tiiii,[24,25] in which four P=O bridging groups connect the phenolic hydroxyls of the resorcinarene scaffold, have been extensively studied in the solid state,[26] in solution,[27,28] and in the gas phase.[29] The main specific interactions responsible for the recognition of methyl ammonium salts evidenced by these studies are H-bonding, cation–dipole and CH_3–π interactions. The removal of the last two interactions upon deprotonation leads to the complete release of the guests as free bases. The potential of cavitand receptors is fully exploited through their surface grafting[30] since the solid surface allows the occurrence of recognition events to otherwise inaccessible solvents,

[a]*Dipartimento di Scienze Chimiche, Università di Catania and INSTM UdR di Catania, v.le A. Doria 6, 95125 Catania, Italy. E-mail: guido.condorelli@unict.it*

[b]*Dipartimento di Chimica, Università di Parma and INSTM UdR di Parma, Parco Area delle Scienze 17/A, 43124 Parma, Italy*

[c]*Dipartimento "G. F. Ingrassia", Università di Catania, Via S.Sofia 87, 95100 Catania, Italy*

[d]*Dipartimento di Chimica "U. Schiff", Università di Firenze and INSTM UdR Firenze, via della Lastruccia 3-13, Sesto Fiorentino, 50019 Firenze, Italy*

[e]*CNR-ISTM, via C. Golgi 19, 20133 Milano, Italy*

precluded by Tiiii insolubility in them. Tiiii surface grafting on silicon slides recently allowed the use of this hydrophobic receptor in the detection of sarcosine, the *N*-methylated analogue of glycine which was indicated as a prostate cancer biomarker,[31] directly in biological fluids (urine).[32]

In the present work, Fe_3O_4 MNPs have been synthesized through a co-precipitation method, and then functionalized with Tiiii and polyethylene glycol (PEG). The aim was to introduce Tiiii recognition properties in a system suited for "*in vivo*" applications (drug delivery) made of superparamagnetic and biocompatible PEGylated MNPs, through an efficient synthetic route. The synthetic approach is based on MNP pre-functionalization with the alkynyl-phosphonic monolayer formed by 10-undecynylphosphonic acid (alkyne), followed by the surface reaction *via* "click-chemistry" of the alkyne termination of the monolayer with the tetraphosphonate cavitand (Tiiii-N_3) and a PEG (PEG-N_3), both bearing an azide moiety. The copper(I) catalysed azide–alkyne cycloaddition (CuAAC), known as "click chemistry",[33] involves 1,3-dipolar cycloaddition between azides and terminal alkynes to form 1,2,3-triazoles. This reaction has several advantages for surface functionalization:[34] (1) high chemoselectivity; (2) high yield; (3) no requirement of temperature or pressure control; (4) easy accessibility of the two active functional groups (azide and alkyne groups) and (5) an irreversible nature that results in a stable linkage, because of the formation of a 1,2,3-triazole ring. Two different types of MNPs functionalized with Tiiii and PEG (Tiiii–PEG–Alkyne@MNPs) were obtained using PEG oligomers with a molecular weight (MW) either of 1000 or 5000 daltons. PEG was introduced onto MNPs to overcome water solubility problems of Tiiii-coated MNPs due to the Tiiii hydrophobic cavity. In addition, PEG coatings reduce reticuloendothelial system (RES) clearance, reduce toxicity, decrease enzymatic degradation, and can thereby increase the stability of nanoparticles, prolonging their circulation half-life *in vivo*.[15,35] The obtained Tiiii and PEG (1000 or 5000 Da) decorated MNPs (Tiiii–PEG–Alkyne@MNPs) were characterized by X-ray photoelectron spectroscopy (XPS) and FTIR spectroscopy. Biocompatibility of Tiiii–PEG–Alkyne@MNPs was measured and compared using two different cell lines, LoVo (human colon adenocarcinoma cell line) and BM18 (mesenchyme cell line). The ability of Tiiii-functionalized nanoparticles to carry *N*-methylated drugs as salts and slowly release them as free bases has been tested adopting procarbazine hydrochloride (PCZ·HCl), a useful anti-neoplastic agent in the treatment of several malignancies,[36] and epinephrine hydrochloride (EPN·HCl), a catecholamine neurotransmitter (known as adrenaline) in mammalian central nervous systems, which is also used to treat various pathologic conditions.[37]

Experimental section

Materials

Iron(II) chloride tetrahydrate ($FeCl_2 \cdot 4H_2O$), iron(III) chloride hexahydrate ($FeCl_3 \cdot 6H_2O$), ammonium hydroxide (NH_4OH), *N*,*N*-dimethylformamide (DMF), ethanol, (+)-sodium L-ascorbate, copper sulphate ($CuSO_4$), methoxypolyethylene glycol azides (PEG-N_3) of molecular weight (MW) 1000 and 5000 Da, PCZ·HCl and EPN were purchased from Sigma-Aldrich Chemicals and were used without further purification. 10-Undecynylphosphonic acid (alkyne) was obtained from SiKÉMIA, Montpellier, France. The water was of Milli-Q grade (18.2 MΩ cm) and was filtered through a 0.22 μm filter.

Synthesis of Tiiii-N_3. Tiiii-N_3 was prepared following a published procedure.[38]

Synthesis of magnetic nanoparticles. Bare magnetite nanoparticles were synthesized by alkaline coprecipitation of Fe^{3+} and Fe^{2+} according to the protocol described in the literature.[39] Briefly, $FeCl_2 \cdot 4H_2O$ and $FeCl_3 \cdot 6H_2O$ (molar ratio 1 : 2) were dissolved in water (50 mL) under a N_2 atmosphere with vigorous stirring. NH_4OH (5 mL, 25%) was added to the solution at 80°, and the reaction was continued for 30 min. The resulting suspension was cooled to room temperature and washed with ultrapure water. The obtained bare magnetic nanoparticles (bare MNPs) were isolated from the solvent by magnetic decantation.

Alkyne-functionalized MNPs. MNPs (200 mg) were dispersed in DMF (25 mL) using an ultrasonic bath for 30 min. An excess of 10-undecynylphosphonic acid (200 mg) was added and the suspension was agitated for 6 h at room temperature. The particles were separated magnetically and washed four times with DMF followed by ethanol and dried under air.

Tiiii-N_3 and PEG-N_3 "click reaction" on MNPs. Alkyne@MNPs (0.1 g), Tiiii-N_3 (0.02 mmol) and PEG-N_3 (0.02 mmol) were dispersed in DMF (20 mL), then $CuSO_4$ (0.01 mmol) and (+)-sodium L-ascorbate (0.05 mmol) were added in sequence. The mixture was vibrated with an orbital shaker at 25 °C for 24 hours. Afterwards, Tiiii–PEG–Alkyne@MNPs were separated with the help of a magnet and washed with DMF three times and ethanol once, then dried overnight at 25 °C. The possible presence of residual copper physisorbed on the MNP surface was ruled out by XPS analysis, since spectra of functionalized MNPs did not show any significant signal in the Cu 2p region (925–960 eV).

Characterization

Chemical characterization. X-Ray powder diffraction (XRD) measurements were performed with a θ–θ 5005 Bruker-AXS diffractometer (Zeiss, Oberkochen, Germany) using Cu Kα radiation operating at 40 kV and 30 mA.

XPS spectra were recorded with a PHI 5600 multi-technique ESCA-Auger spectrometer with a standard Mg-Kα X-ray source. Analyses were carried out with a photoelectron angle of 45° (relative to the sample surface) with an acceptance angle of ±7°. The XPS binding energy (B.E.) scale was calibrated by centering the C 1s peak due to hydrocarbon moieties and adventitious carbon at 285.0 eV. Transmission FT-IR measurements were recorded with a JASCO FTIR 430 spectrometer, using the KBr pellet technique, with 100 scans collected per spectrum (scan range 560–4000 cm^{-1}, resolution 4 cm^{-1}).

Dynamic light scattering (DLS) and zeta-potential measurements of MNPs were performed with a Nano Zetasizer (Malvern Instruments, Malvern, UK).

TEM characterization. Average nanoparticle diameter and size distribution of Tiiii–PEG–Alkyne@MNPs were determined by Transmission Electron Microscopy (TEM), using a CM12 PHILIPS microscope operating at 100 kV. Samples were prepared by drop drying an aqueous diluted suspension of MNPs onto 200 mesh carbon-coated copper grids. Recorded images were further analysed with the Image Pro-Plus© software. The mean diameter and size distribution of each sample were obtained from a statistical analysis over 400 nanoparticles.

Magnetic characterization. Magnetic measurements were carried out by a SQUID magnetometer (Quantum Design MPMS) operating in the 1.8–300 K temperature range with applied field up to 5 T. Measurements were performed on dried powder, hosted in a Teflon sample holder and then pressed in a pellet in order to prevent preferential orientation of the nanocrystallites under the magnetic field action. All data were corrected for the diamagnetic contribution of the sample holder. ZFC/FC curves were obtained by cooling the sample in the absence/presence of a small magnetic field from room temperature to 5 K, then measuring the magnetic moment on warming the sample to 300 K with a controlled rate with a small probe field applied (5 mT).

Cytotoxicity of Tiiii–PEG–Alkyne@MNPs. Human mesenchymal stem cells (hMSCs), obtained from human bone marrow of healthy donors, and human colon adenocarcinoma (LoVo) were cultivated, respectively, in α-Minimum Essential Medium (αMEM) and RPMI 1640 supplemented with L-glutamine, nucleosides, Fungizon (penicillin 10 000 U mL^{-1}, streptomycin 1000 μg mL^{-1}), 10% fetal bovine serum (FBS), and 100 μM ascorbic acid and maintained in a 37 °C incubator, in a humidified atmosphere of 5% CO_2/95% air. All products used were purchased from GIBCO (Life technologies).

Both cell lines were detached by Trypsin/EDTA·4Na (0.05%/1×) and used for experiments. From a 10^4 cells per mL cell suspension, 200 μL was seeded into each well of a 96-well tissue culture plate and incubated for 24 h followed by a medium change with fresh medium containing Tiiii–PEG–Alkyne@MNPs at concentrations of 20, 40, and 80 μg mL^{-1}. After incubation for 24, 48 and 72 h, cytotoxicity assay was performed using an MTT test, based on reduction of tetrazolium salts to formazan by mitochondrial dehydrogenase. The optical density (OD) values at 550 nm of the wells, with background subtraction of OD at 655 nm, were measured by a microliter plate reader. The cell viability was expressed in values % with respect to the control. All experiments were performed in triplicate.

Drug loading and release study. Stock solutions of PCZ (1 mM) and EPN hydrochlorides (1 mM) were prepared by dissolving the drugs in Phosphate Buffered Saline (PBS) water solution. PBS was obtained by mixing Na_2HPO_4 (40.6 mg) and NaH_2HPO_4 (85.6 mg) in water (100 mL) (pH 6.8, 10 mM). The adopted pH is in the low edge of the physiological range (6.8–7.4) suited for normal cells and is close to extracellular pH values (6.5–6.9) observed for malignant tumors.[40] Drug loading was performed by dispersing MNPs (5 mg, Tiiii–PEG–Alkyne@MNPs) in PCZ·HCl solution (4 mL) or EPN·HCl solution (4 mL). The solution was sonicated for 1 h in an ultrasonic bath, and the MNPs were isolated from the solution by magnetic separation. The amount of loaded drug was determined by UV-Vis measurements of the drug solutions before and after loading. The PCZ-loaded and EPN-loaded MNPs were suspended in PBS and were transferred into dialysis tubing (MW cutoff 3.0 kDa) and dialyzed against PBS (50 mL) for 36 h. Samples (2 mL) were periodically removed and assayed. The withdrawn volume of each sample was replaced by the same volume of fresh medium. The amounts of released PCZ and EPN were analysed with a JASCO V-560 UV/Vis spectrophotometer equipped with a 1 cm path length cell at 230 nm and 300 nm respectively. The drug release study was performed in duplicate.

Results and discussion

The structure and crystallinity of the bare MNPs were investigated by powder X-ray diffractometry (Fig. 1). The position and relative intensity of all diffraction peaks (2θ reflections: 30.1, 35.5, 43.1, 57.0, 62.7°) well matched those of the standard PDF cards for magnetite (19-0629), maghemite (39-1346) or any intermediate composition between the two phases, and could be indexed as (220), (311), (400), (511) and (440), respectively. The lattice constant, a, was found to be 8.378 Å, close to the lattice parameter of bulk magnetite (8.396 Å). The small discrepancy can be ascribed to a slight oxidation of surface ferrous ions. The crystallite size has been evaluated at the full-width at half maximum of the strongest reflection of the (311) peak, using the Debye–Scherrer equation ($D = 0.9\lambda/\beta \cos \theta$), where D is the average crystallite size (nm), λ is the X-ray wavelength (nm), θ and β are the Bragg angle (radians) and the excess line broadening (radians), respectively. The average particle size for bare MNPs is about 12 nm.

The two-step synthetic route to obtain Tiiii–PEG–Alkyne@MNPs is illustrated in Scheme 1. In order to covalently immobilize the Tiiii cavitand and PEG on the MNP surface through CuAAC reaction, MNPs functionalized with monolayers having terminal acetylenic groups have been firstly prepared. Therefore a phosphonic acid, able to covalently anchor on the MNP surface through P–O–Fe bonds and bearing a terminal acetylene group, was grafted on MNPs (Alkyne@MNPs) in the first step. Tiiii and PEG molecules (either with MW 1000 or 5000 Da) bearing an azide group were bonded on alkyne pre-functionalized MNPs using Cu(I)-catalyzed 1,3-dipolar cycloaddition reaction.

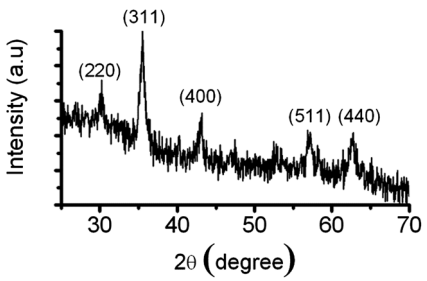

Fig. 1 XRD pattern of bare MNPs.

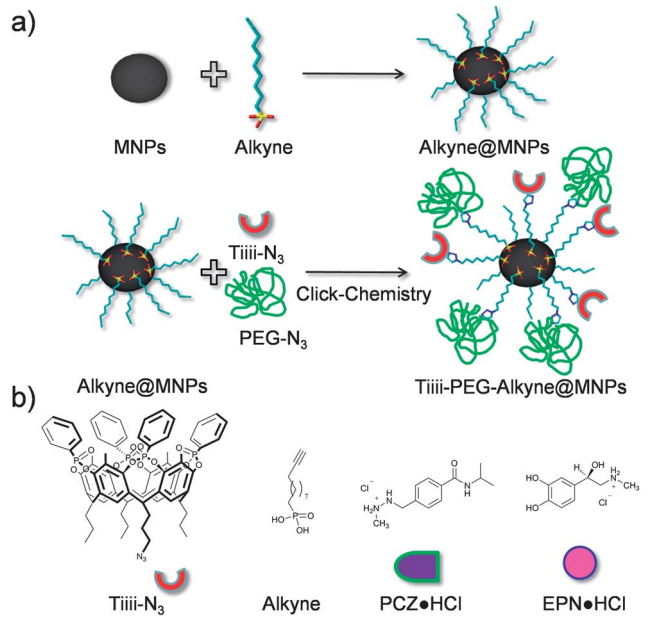

Scheme 1 (a) Reaction steps for the preparation of functionalized-MNPs; (b) structure of cavitand, phosphonic acid grafting agent and the drugs used in their complexed salt form.

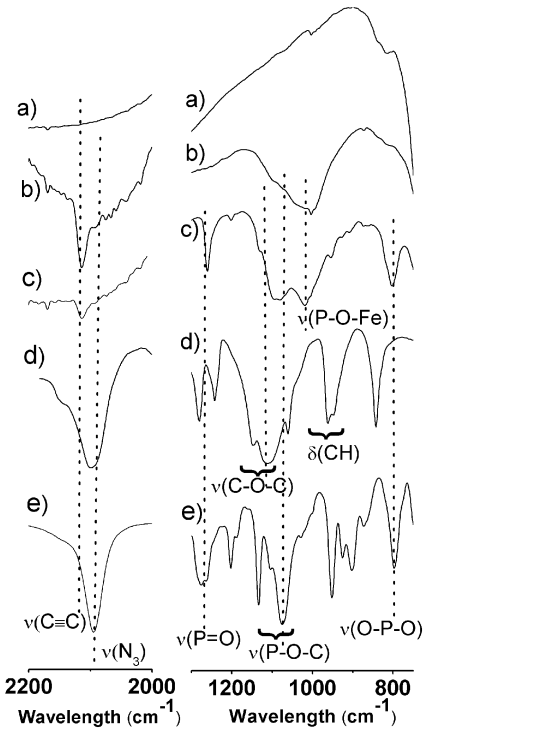

Fig. 2 FT-IR spectral regions in the 2000–2200 cm^{-1} (left) and 750–1300 cm^{-1} (right) ranges of (a) bare MNPs, (b) Alkyne@MNPs, (c) Tiiii–PEG–Alkyne@MNPs, (d) PEG-N_3, and (e) Tiiii-N_3.

All MNPs obtained in the first and second steps, Alkyne@MNPs and Tiiii–PEG–Alkyne@MNPs, have been characterized by XPS and FTIR. Note, however, that since characterizations of MNPs obtained adopting either PEG 1000 Da or PEG 5000 Da are similar, only XPS and FTIR spectra of Tiiii–PEG(1000 Da)–Alkyne@MNPs are reported, although results are valid for both PEG 1000 Da and 5000 Da.

Fig. 2 shows the FT-IR spectra in the 750–1300 cm^{-1} (right) and in the 2200–2000 cm^{-1} region (left) of bare MNPs, Alkyne@MNPs, Tiiii–PEG–Alkyne@MNPs, and the powders of Tiiii-N_3 and PEG-N_3. In the FT-IR spectrum of Alkyne@MNPs, the absence of the P═O stretches (1254 cm^{-1}) and P–O–H stretches (920 cm^{-1}) typical of phosphonic acid powders[16,25,41] and the presence of a single broad and strong band at *ca.* 1040 cm^{-1} due to the phosphate bonding group indicate that the phosphonic acids anchor through multidentate bonding with the surface,[16] which involves both P═O and P–O-terminations. FT-IR spectra of Tiiii–PEG–Alkyne@MNPs show the increase of a broad band between 1150 and 1050 cm^{-1} due to the presence of P–O–C of the cavitand and the overlapped C–O–C stretching of PEG. In addition, we can observe the presence of new features at 1256 cm^{-1} and 803 cm^{-1} due to the free P═O stretches and O–P–O vibrations of the Tiiii cavitand, respectively. In the FT-IR spectra of Alkyne@MNPs the presence of the characteristic absorption peak of the alkyne group at 2108 cm^{-1}, which is absent in the spectra of bare MNPs, suggests that the anchoring process preserves the active alkyne terminated groups.[42] After the subsequent click chemistry reaction, in Tiiii–PEG–Alkyne@MNP spectra, the decrease of this alkyne characteristic band indicates the successful proceeding of "click reaction". Furthermore, the absence of stretching vibration of azido groups at 2075 cm^{-1} in the spectrum of Tiiii–PEG–Alkyne@MNPs ruled out any possible physisorption of Tiiii-N_3 or PEG-N_3 on the MNP surface.

XPS P 2p, N 1s, C 1s and O 1s spectral regions of (a) Alkyne@MNPs and (b) Tiiii–PEG–Alkyne@MNPs are shown in Fig. 3. The presence and the position of the P 2p band is a reliable indicator to evaluate the grafting process of the phosphonic acid. The P 2p peak of Alkyne@MNPs is observed at 133.2 eV (Fig. 3). This value, which is about 0.9 eV lower than the value observed for undissociated $-PO_3H_2$ groups, is associated with the deprotonation of –POH terminations, which leads to the occurrence of two P–O–Fe bonds. After Tiiii and PEG grafting, the P 2p band of Tiiii–PEG–Alkyne@MNPs (Fig. 3) is still centered at 133.2 eV, thus indicating that the anchored phosphonic acid is not removed by the click reaction. However, the band shape shows a broadening towards higher B.E. which can be explained by the presence of the expected component around 134 eV due to the tetraphosphonic bridge of Tiiii. The N 1s spectral regions of Alkyne@MNPs and Tiiii–PEG–Alkyne@MNPs are shown in Fig. 3. As expected, no N 1s signal is present on Alkyne@MNPs, whilst a N 1s peak centered at 401 eV is observed after click reaction. The band shape is broad, suggesting the presence of different nitrogen atoms consistently with the formation of a triazole moiety from the fusion of azido species with the acetylene-decorated surface. The N 1s signal can be deconvolved into two peaks due to N–N*═N* (N* at 400.2 eV) and N*–N═N (N* at 401.7 eV) with a 2 : 1 intensity ratio.[43] No signal was present at 405 eV, corresponding to the central, electron deficient N atom of the azido group, thus

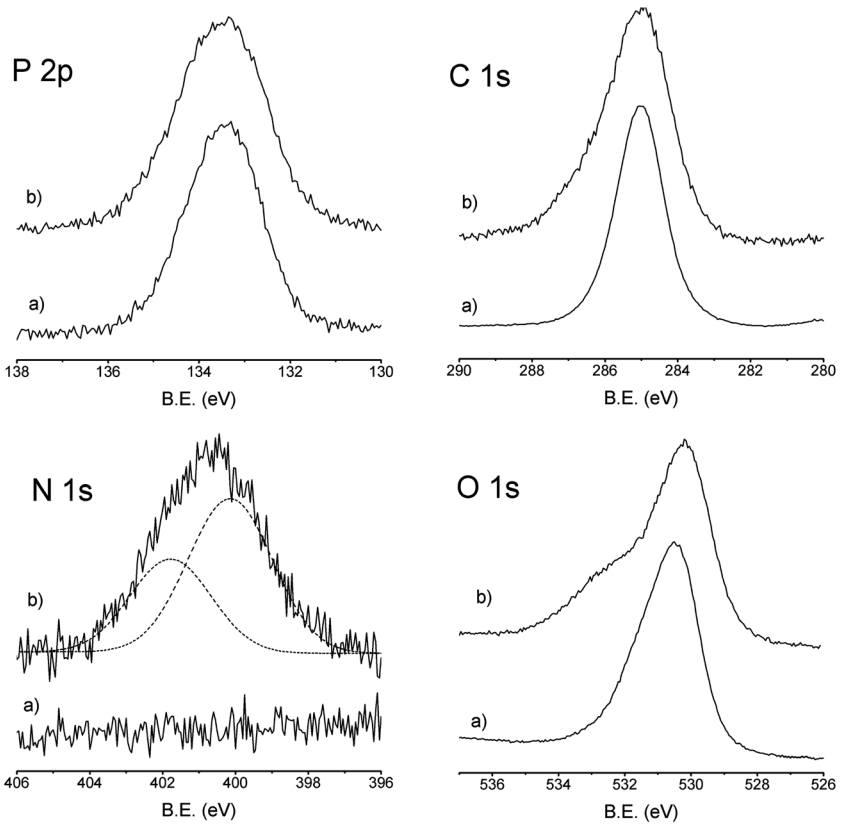

Fig. 3 High resolution P 2p, N 1s, C 1s and O 1s XPS spectral regions of (a) Alkyne@MNPs and (b) Tiiii–PEG–Alkyne@MNPs.

indicating that no physisorption of Tiiii-N_3 or PEG-N_3 occurs. In the high-resolution C 1s region (Fig. 3) of Alkyne@MNPs is present a single contribution at 285.0 eV, assigned only to aliphatic carbons. In the spectra of Tiiii–PEG–Alkyne@MNPs beside the main peak at 285.0 eV due to aliphatic and aromatic carbons, there is an evident shoulder around 286 eV due to the presence of the oxygen-bonded carbons of Tiiii and PEG.[44] In addition, quantitative XPS analysis indicates a significant increase of the C amount on the surface in Tiiii–PEG–Alkyne@MNPs.

O 1s XPS spectra of Alkyne@MNPs (Fig. 3) mainly consist of a component at 530.2 eV due to the iron oxide cores. After the addition of Tiiii and PEG a new component at 532.2 eV becomes evident due to the PEG oxygens.

On the basis of the overall XPS and FTIR results, it could be concluded that Tiiii-N_3 and PEG-N_3 have been successfully grafted on Alkyne@MNPs through click chemistry reaction.

In Fig. 4 a typical TEM micrograph of the Tiiii–PEG–Alkyne@MNPs is shown. The sample is composed of almost spherical nanoparticles with a mean diameter of 10.8 ± 3.5 nm. The diameter size distribution obtained from a statistical analysis over *ca.* 400 nanoparticles, reported in the inset of Fig. 4, can be nicely fitted to a log-normal function, as commonly observed for nanoparticles prepared with wet-chemical techniques. The best fit parameters give a mean diameter of 10.3 nm ($\sigma = 0.32$), which is in agreement with the value obtained from direct statistics.

The magnetic properties of Tiiii–PEG–Alkyne@MNPs were investigated both as a function of temperature and magnetic field. In Fig. 5a are reported the zero-field cooled (ZFC) and field-cooled (FC) magnetizations as a function of temperature: the sample shows thermal irreversibility characteristic of an ensemble of single domain MNPs of a few tens of nanometers. However, the blocking temperature, T_B, commonly identified as the maximum of the ZFC curve, is higher than room temperature and is clearly not reached in the investigated temperature range.

In Fig. 5b are reported the *M vs. H* curves recorded at low temperature (2.5 K) and at room temperature (300 K). At low temperature, the magnetization curve shows hysteresis (see magnification in the inset of Fig. 5b) with a coercive field of $\mu_0 H_C = 26.7$ mT and a remnant magnetization, $M_R = \frac{M_{0\,T}}{M_{5\,T}}$, of 0.39. This value is slightly lower than the one expected for a set of isolated uniaxial nanoparticles whose easy axis is isotropically orientated (0.5), a behaviour that is commonly observed in iron oxide NPs and can be also influenced by the presence of magnetic interparticle interactions.[45] At room temperature (300 K), neither hysteresis nor coercivity was observed. The saturation magnetization values, M_S, estimated by fitting the curve to the empirical law,[46] $M = M_S + \frac{a}{H} + \frac{b}{H^2}$, at high fields, are 75 and 67 emu g^{-1}, for 2.5 and 300 K, respectively, which are *ca.* 25% smaller than those observed for bulk magnetite,[47]

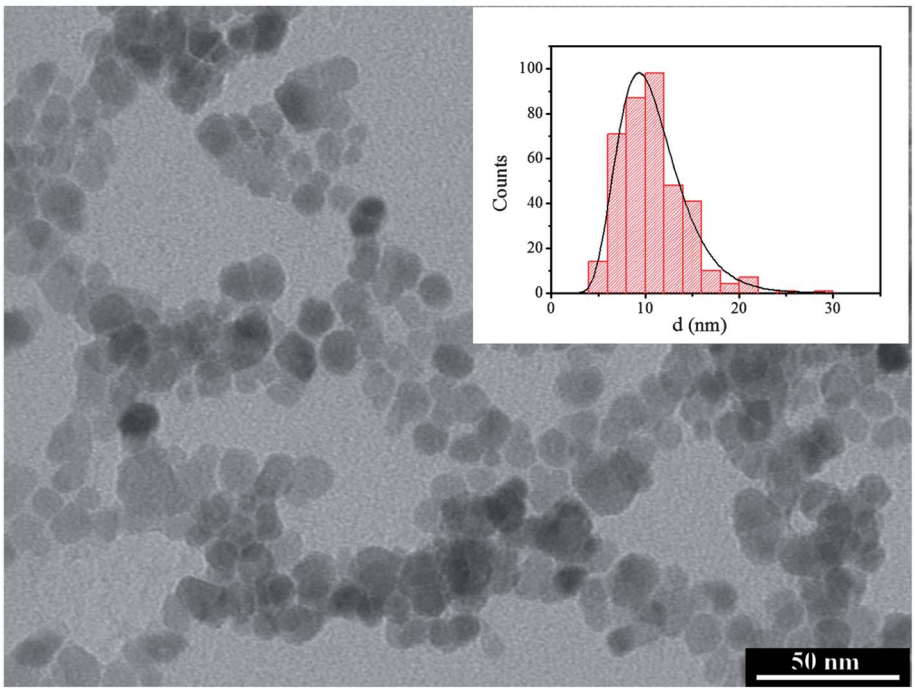

Fig. 4 TEM image of Tiiii–PEG–Alkyne@MNPs. In the inset, the size distribution over *ca.* 400 nanoparticles is reported; the continuous line represents the best fit curve to a log-normal distribution.

although quite large if compared to the data reported in the literature for nanosized iron oxides. The reduction of M_S in nanosized magnetic materials can be attributed to the presence of a dead spin layer on the surface,[48] whose contributions become more and more significant with size reduction.

The effective magnetic anisotropy constant, K_{eff}, evaluated from the low temperature magnetization curve as $K_{eff} = \frac{H_C M_S}{0.96}$ is 9.6 kJ m^{-3} which is in good agreement with the value of bulk magnetite (11.0 kJ m^{-3}).[48]

The mean hydrodynamic sizes of functionalized MNPs were determined by DLS in PBS (pH 6.8) (Fig. 6a). The hydrodynamic size distributions of Tiiii–PEG–Alkyne@MNPs coated with PEG 1000 or 5000 Da were centered at 70 nm and 80 nm, respectively. However, the broadening of the size distribution towards larger values in Tiiii–PEG(1000)–Alkyne@MNPs suggests the occurrence of some aggregations for low MW coating. Note that a comparison with the hydrodynamic size of naked Fe_3O_4 NPs in PBS was not possible since severe aggregation was observed at pH = 6.8, which is very close to the Fe_3O_4 isoelectric point (pH = 6.2). The hydrodynamic size of naked MNPs obtained in alkaline solution (pH = 11) was 70 nm. The zeta potential of both Tiiii–PEG–Alkyne@MNPs coated with PEG 1000 or 5000 Da was determined as a function of the pH (Fig. 6b). Zeta potential *vs.* pH trends are similar for the two PEGs with different lengths (1000 or 5000 Da), with close isoelectric points (at pH = 2.4 and 2.9 for PEG 5000 and 1000 Da, respectively) and a zeta potential in the physiologic pH range around −30 mV. The low values on the isoelectric points and, therefore, the negative values of the zeta potential in the physiological pH range, are mainly due to

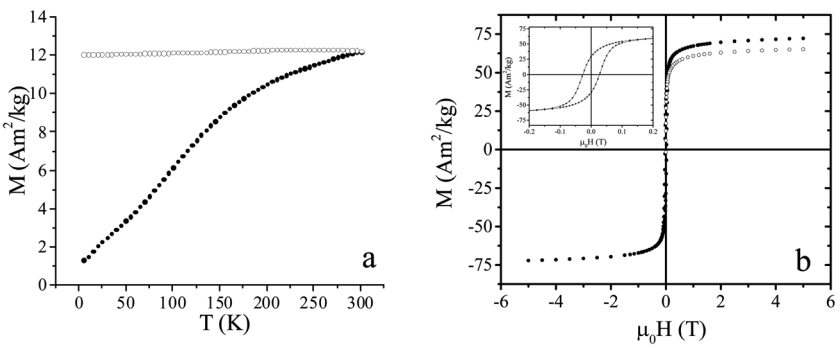

Fig. 5 (a) Temperature dependence of the ZFC (full circles) and FC (open circles) magnetizations of Tiiii–PEG–Alkyne@MNPs, measured at the field of 5 mT; (b) *M vs. H* curves of Tiiii–PEG–Alkyne@MNPs, measured at 2.5 K (full circles) and 300 K (open circles). In the inset of (b) is reported the low temperature curve magnification in the low field region.

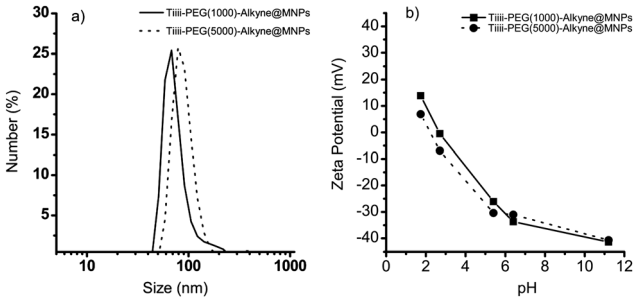

Fig. 6 (a) Size distribution in PBS and (b) zeta potential as a function of pH of Tiiii–PEG–Alkyne@MNPs coated with PEG 1000 (solid line) or 5000 Da (dashed line).

the negatively charged core and the effect of the phosphonic acid prefunctionalization which further shifts the isoelectric point to lower values.[20]

The evaluation of cell viability of Tiiii–PEG–Alkyne@MNPs coated with PEG (5000 or 1000 Da) is reported in Fig. 7. The values obtained at 72 h showed a different reduction of MTT depending on the nanoparticles coating and on the type of cell line used. The cell viability of mesenchymal cells was unchanged for all investigated concentrations of nanoparticles. Conversely, in LoVo cells, a slight decrease compared to the control was observed. The decrease was similar for all three concentrations and it was more evident using Tiiii–PEG(1000)–Alkyne@MNPs.

Therefore, both nanocarriers were shown to be biocompatible with hMSCs at all concentrations, while they showed a lower biocompatibility in LoVo cells to which they caused a slowdown in proliferative activity.

Drug loading and release experiments were performed by adopting two *N*-methylated molecules: the antitumor drug PCZ which is an alkylating agent and the neurotransmitter EPN. Molecule loading was performed in PBS (1 h of treatment) from their hydrochloride solutions (1 mM) which allow enough amounts of protonated guests suitable for Tiiii complexation (Scheme 2). Drug loading/release of Tiiii receptors is in fact mainly affected by the protonation/deprotonation equilibrium of the guest.[26,27]

The amounts of loaded drugs were 5.4 μg mg^{-1} (21 μmol g^{-1}) and 8.3 μg mg^{-1} (38 μmol g^{-1}) for PCZ and EPN, respectively. These values are comparable to other drug loads such as doxorubicin (15–150 μmol g^{-1})[49,50] and 5-fluorouracil (6–90 μmol g^{-1}).[51]

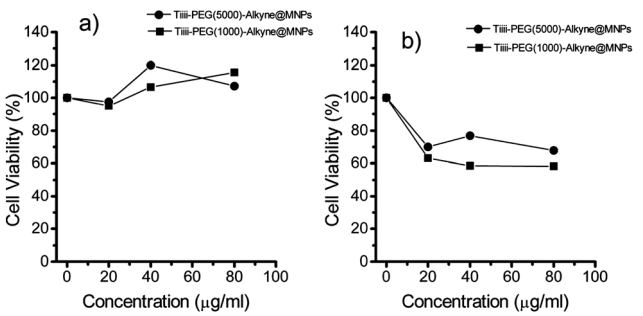

Fig. 7 (a) Cell viability of hMSC cells with Tiiii–PEG–Alkyne@MNPs coated with PEG (1000 or 5000 Da) and (b) cell viability of LoVo cells with Tiiii–PEG–Alkyne@MNPs coated with PEG (1000 or 5000 Da).

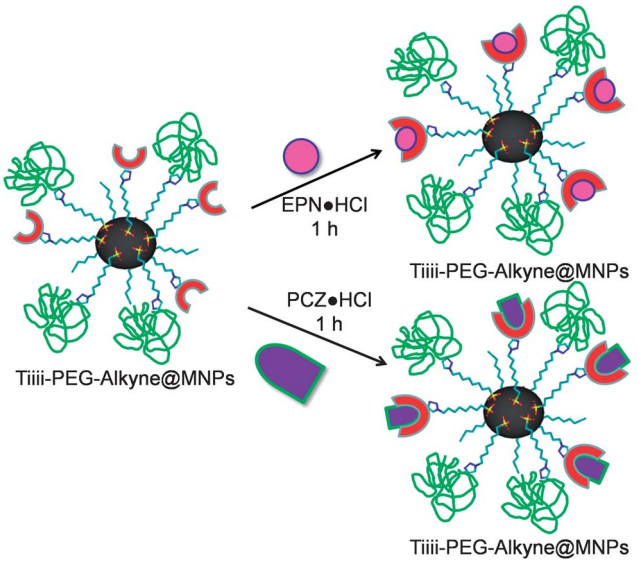

Scheme 2 Drug-loading of Tiiii–PEG–Alkyne@MNPs.

For release experiments, drug-loaded MNPs are first magnetically separated and then re-dispersed in fresh PBS water solution, loaded drugs are released from the Tiiii cavity through guest deprotonation equilibrium.[26,27]

Fig. 8 shows the release profile of PCZ and EPN from Tiiii–PEG–Alkyne@MNPs. It was evident after 36 hours that almost 96% of PCZ loaded was released, while EPN release is around 80%, both as free bases. The release profile of PCZ is much faster than EPN, with almost 50% of release after 2 h of experiment; at the same time the EPN release is around 35%. The great amount and the fast release profile of PCZ, with respect to the EPN release profile, can be justified considering the medium where the experiment was performed. PCZ is freely soluble in water and the release is improved, while EPN is sparingly soluble in water and the release is slower and not complete. Although the interaction between the Tiiii cavity and the $^{+}NH_2$–CH_3 group is the same irrespective of the R group attached,[28,32] it is solvent dependent. In this case the higher solubility of PCZ in PBS is responsible for faster release.

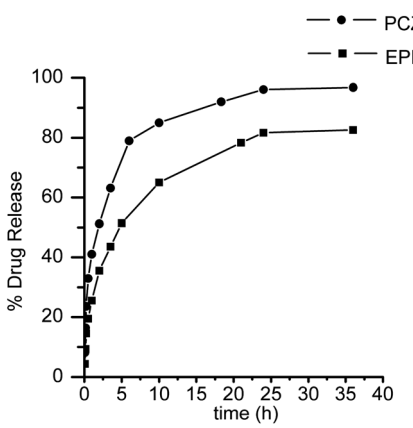

Fig. 8 PCZ and EPN release profile from Tiiii–PEG–Alkyne@MNPs.

Conclusions

In this paper we reported on the synthesis of new multifunctional nanoparticles possessing magnetic, biocompatibility and drug load/release capabilities. The developed synthetic approach is based on MNPs pre-functionalization with a phosphonic linker followed by covalent anchoring of biocompatible PEG chains and Tiiii receptors. Overall FT-IR and XPS characterizations demonstrated the success of the adopted synthetic route. Obtained MNPs (mean diameter 10 nm) show the typical magnetic behaviour of an ensemble of single domain magnetite nanoparticles, with magnetic irreversibility at low temperature and no coercivity at 300 K. The main magnetic parameters are consistent with those of magnetite nanoparticles of a few tens of nanometers with a broad size distribution, even if narrower than those of most commonly used commercial ones. Due to their good crystallinity level, the obtained values of saturation magnetization are high, making this nanomaterial suitable for the most common biomedical applications such as contrast agents for MRI or heat mediators for MFH.

Moreover, cytotoxicity tests indicate that the functional MNPs could be applied in biomedical or bioengineering field. In addition, the presence of hydrophilic PEG chains allowed overcoming water solution problems associated with the hydrophobic Tiiii receptors. Although both Tiiii–PEG–Alkyne@MNPs with 1000 Da or 5000 Da PEG were biocompatible, better properties were observed adopting 5000 Da PEG. Despite the presence of the long PEG chains, the Tiiii receptors anchored on the MNP surface retain their peculiar complexation properties. Drug release experiments showed that both Tiiii–PEG–Alkyne@MNPs with 5000 and 1000 Da PEG can be loaded with *N*-methylated molecules of interest in the biomedical fields. In particular, the antitumoral drug PCZ and the neurotransmitter EPN have been used as tested molecules, but the applications of these MNPs can be extended to the loading and recognition of several *N*-methylated salts, such as *N*-methylated aminoacids, due to the specific recognition properties of Tiiii receptors.

Acknowledgements

The authors thank Ministero dell'Istruzione, dell'Università e della Ricerca (MIUR) for financial support through FIRB "RINAME Rete Integrata per la NAnoMEdicina" (RBAP114AMK). The authors also thank Prof. G. Vecchio for DLS facilities.

References

1 M. Colombo, S. Carregal-Romero, M. F. Casula, L. Gutiérrez, M. P. Morales, I. B. Böhm, J. T. Heverhagen, D. Prosperi and W. J. Parak, *Chem. Soc. Rev.*, 2012, **41**, 4306–4334.
2 G. Mistlberger, K. Koran, E. Scheucher, D. Aigner, S. M. Borisov, A. Zankel, P. Polt and I. Klimant, *Adv. Funct. Mater.*, 2010, **20**, 1842–1851.
3 J. Nicolas, S. Mura, D. Brambilla, N. Mackiewicz and P. Couvreur, *Chem. Soc. Rev.*, 2013, **42**, 1147–1235.
4 Y. Pan, X. Du, F. Zhao and B. Xu, *Chem. Soc. Rev.*, 2012, **41**, 2912–2942.
5 N. Lee and T. Hyeon, *Chem. Soc. Rev.*, 2012, **41**, 2575–2589.
6 F. Hu and Y. S. Zhao, *Nanoscale*, 2012, **4**, 6235–6243.
7 Y. Huang, S. He, W. Cao, K. Cai and X.-J. Liang, *Nanoscale*, 2012, **4**, 6135–6149.
8 S. Jiang, K. Y. Win, S. Liu, C. P. Teng, Y. Zheng and M.-Y. Han, *Nanoscale*, 2013, **5**, 3127–3148.
9 N. Erathodiyil and J. Y. Ying, *Acc. Chem. Res.*, 2011, **44**, 925–935.
10 S. Laurent, D. Forge, M. Port, A. Roch, C. Robic, L. V. Elst and R. N. Muller, *Chem. Rev.*, 2008, **108**, 2064–2110.
11 W. Wang, V. Pacheco, H.-J. Krause, Y. Zhang, H. Dong, R. Hartmann, D. Willbold, A. Offenhäusser and Z. Gu, *J. Phys. Chem. C*, 2012, **116**, 17880–17884.
12 S. T. Selvan, T. T. Y. Tan, D. K. Yi and N. R. Jana, *Langmuir*, 2010, **26**, 11631–11641.
13 A. K. Gupta and M. Gupta, *Biomaterials*, 2005, **26**, 3995–4021.
14 M. Mazur, A. Barras, V. Kuncser, A. Galatanu, V. Zaitzev, K. V. Turcheniuk, P. Woisel, J. Lyskawa, W. Laure, A. Siriwardena, R. Boukherroub and S. Szunerits, *Nanoscale*, 2013, **5**, 2692–2702.
15 E. K. U. Larsen, T. Nielsen, T. Wittenborn, L. M. Rydtoft, A. R. Lokanathan, L. Hansen, L. Østergaard, P. Kingshott, K. A. Howard, F. Besenbacher, N. C. Nielsen and J. Kjems, *Nanoscale*, 2012, **4**, 2352–2361.
16 C. Tudisco, V. Oliveri, M. Cantarella, G. Vecchio and G. G. Condorelli, *Eur. J. Inorg. Chem.*, 2012, **32**, 5323–5331.
17 C. Tassa, S. Y. Shaw and R. Weissleder, *Acc. Chem. Res.*, 2011, **44**, 842–852.
18 I. J. Bruce and T. Sen, *Langmuir*, 2005, **21**, 7029–7035.
19 C. Yee, G. Kataby, A. Ulman, T. Prozorov, H. White, A. King, M. Rafailovich, J. Sokolov and A. Gedanken, *Langmuir*, 1999, **15**, 7111–7115.
20 S. Mohapatra and P. Pramanik, *Colloids Surf., A*, 2009, **339**, 35–42.
21 K. V. P. M. Shafi, A. Ulman, X. Yan, N.-L. Yang, C. Estournès, H. White and M. Rafailovich, *Langmuir*, 2001, **17**, 5093–5097.
22 B. Basly, G. Popa, S. Fleutot, B. P. Pichon, A. Garofalo, C. Ghobril, C. Billotey, A. Berniard, P. Bonazza, H. Martinez, D. Felder-Flesch and S. Begin-Colin, *Dalton Trans.*, 2013, **42**, 2146–2157.
23 D. J. Cram and J. M. Cram, in *Container Molecules and Their Guests*, ed. J. F. Stoddart, The Royal Society of Chemistry, Cambridge, 1994.
24 R. Pinalli, M. Suman and E. Dalcanale, *Eur. J. Org. Chem.*, 2004, **3**, 451–462.
25 R. Pinalli and E. Dalcanale, *Acc. Chem. Res.*, 2013, **46**, 399–411.
26 E. Biavardi, M. Favazza, A. Motta, I. L. Fragalà, C. Massera, L. Prodi, M. Montalti, M. Melegari, G. G. Condorelli and E. Dalcanale, *J. Am. Chem. Soc.*, 2009, **131**, 7447–7455.
27 E. Biavardi, G. Battistini, M. Montalti, R. M. Yebeutchou, L. Prodi and E. Dalcanale, *Chem. Commun.*, 2008, 1638–1640.
28 R. M. Yebeutchou and E. Dalcanale, *J. Am. Chem. Soc.*, 2009, **131**, 2452–2453.
29 E. Kalenius, D. Moiani, E. Dalcanale and P. Vainiotalo, *Chem. Commun.*, 2007, 3865–3867.
30 G. G. Condorelli, A. Motta, M. Favazza, I. L. Fragalà, M. Busi, E. Menozzi and E. Dalcanale, *Langmuir*, 2006, **22**, 11126–11133.

31 A. Sreekumar, L. M. Poisson, T. M. Rajendiran, A. P. Khan, Q. Cao, J. Yu, B. Laxman, R. Mehra, R. J. Lonigro, Y. Li, M. K. Nyati, A. Ahsan, S. Kalyana-Sundaram, B. Han, X. Cao, J. Byun, G. S. Omenn, D. Ghosh, S. Pennathur, D. C. Alexander, A. Berger, J. R. Shuster, J. T. Wei, S. Varambally, C. Beecher and A. M. Chinnaiyan, *Nature*, 2009, **457**, 910–915.
32 E. Biavardi, C. Tudisco, F. Maffei, A. Motta, C. Massera, G. G. Condorelli and E. Dalcanale, *Proc. Natl. Acad. Sci. U. S. A.*, 2012, **109**, 2263–2268.
33 H. C. Kolb, M. G. Finn and K. B. Sharpless, *Angew. Chem., Int. Ed.*, 2001, **40**, 2004–2021.
34 H. Koichiro, M. Makoto, S. Wataru and Y. Toshinobu, *Chem. Mater.*, 2009, **21**, 1318–1325.
35 J.-B. Qu, H.-H. Shao, G.-L. Jing and F. Huang, *Colloids Surf., B*, 2013, **102**, 37–44.
36 C. A. Graham and T. F. Cloughesy, *Semin. Oncol. Nurs.*, 2004, **20**, 260–272.
37 Y. Yamanaka, T. Mammoto, T. Kirita, M. Mukai, T. Mashimo, M. Sugimurac, Y. Kishi and H. Nakamura, *Cancer Lett.*, 2002, **176**, 143–148.
38 M. Dionisio, J. M. Schnorr, V. K. Michaelis, R. G. Griffin, T. M. Swager and E. Dalcanale, *J. Am. Chem. Soc.*, 2012, **134**, 6540–6543.
39 Y. S. Kang, S. Risbud, J. F. Rabolt and P. Stroeve, *Chem. Mater.*, 1996, **8**, 2209–2211.
40 V. Estrella, T. Chen, M. Lloyd, J. Wojtkowiak, H. H. Cornnell, A. Ibrahim-Hashim, K. Bailey, Y. Balagurunathan, J. M. Rothberg, B. F. Sloane, J. Johnson, R. A. Gatenby and R. J. Gillies, *Cancer Res.*, 2013, **73**, 1524–1535.
41 E. Smecca, A. Motta, M. E. Fragalà, Y. Aleeva and G. G. Condorelli, *J. Phys. Chem. C*, 2013, **117**, 5364–5372.
42 W. Zhang, Y. Zhang, X. Shi, C. Liang and Y. Xian, *J. Mater. Chem.*, 2011, **21**, 16177–16183.
43 A. C. Cardiel, M. C. Benson, L. M. Bishop, K. M. Louis, J. C. Yeager, Y. Tan and R. J. Hamers, *ACS Nano*, 2012, **6**, 310–318.
44 R. Tedja, A. H. Soeriyadi, M. R. Whittaker, M. Lim, C. Marquis, C. Boyer, T. P. Davisband and R. Amal, *Polym. Chem.*, 2012, **3**, 2743–2751.
45 M. El-Hilo, R. W. Chantrell and K. O'Grady, *J. Appl. Phys.*, 1998, **9**, 5114–5122.
46 J. I. Gittlemann, B. Abeles and S. Bosowski, *Phys. Rev. B: Solid State*, 1974, **9**, 3891–3897.
47 M. M. Schieber, Iron oxides and their compounds, in *Experimental magnetochemistry*, ed. E. P. Wohlfarth, North-Holland Publishing Company, Amsterdam, 1967.
48 A. Millan, A. Urtizberea, N. J. O. Silva, F. Palacio, V. S. Amaral, V. Snoeck and V. Serin, *J. Magn. Magn. Mater.*, 2007, **312**, L5–L9.
49 M. K. Yu, Y. Y. Jeong, J. Park, S. Park, J. W. Kim, J. J. Min, K. Kim and S. Jon, *Angew. Chem., Int. Ed.*, 2008, **47**, 53–62.
50 T. K. Jain, M. A. Morales, S. K. Sahoo, D. L. Leslie-Pelecky and V. Labhasetwar, *Mol. Pharmaceutics*, 2005, **2**, 194–205.
51 J. L. Arias, F. Linares-Molinero, V. Gallardo and Á. V. Delgado, *Eur. J. Pharm. Sci.*, 2008, **33**, 252–261.

